

THESIS FOR THE DEGREE OF LICENTIATE OF ENGINEERING

# Radar Measurements of Temporal Variation in a Boreal Forest

ALBERT MONTEITH

Department of Space, Earth and Environment  
Division of Microwave and Optical Remote Sensing  
CHALMERS UNIVERSITY OF TECHNOLOGY

Göteborg, Sweden 2018

Radar Measurements of Temporal Variation in a Boreal Forest  
ALBERT MONTEITH

© ALBERT MONTEITH, 2018

Department of Space, Earth and Environment  
Division of Microwave and Optical Remote Sensing  
Chalmers University of Technology  
SE-412 96 Göteborg  
Sweden  
Telephone: +46 (0)31-772 2235

Cover:

The BorealScat radar measurement tower as viewed from one of the trihedral corner reflectors on the ground. Photo: Albert Monteith.

Chalmers Reproservice  
Göteborg, Sweden 2018

Radar Measurements of Temporal Variation in a Boreal Forest  
Thesis for the degree of Licentiate of Engineering  
ALBERT MONTEITH  
Department of Space, Earth and Environment  
Division of Microwave and Optical Remote Sensing  
Chalmers University of Technology

## ABSTRACT

Synthetic aperture radar (SAR) on a satellite platform is a suitable technique for all-weather global monitoring of forest parameters such as biomass. This is important for increasing the accuracy of the global terrestrial carbon flux, the largest uncertainty in our current understanding of the Earth's carbon cycle. In recent decades there has been increasing interest in relating SAR observables from current and future spaceborne SAR missions to forest parameters. Ideally, these SAR observables are only dependent on the forest parameters of interest, but they are also affected by temporal variations in the forest due to weather, diurnal and seasonal changes. These effects are not properly accounted for in current forest parameter estimation models using SAR data due to shortcomings in our understanding of these effects.

To fill this knowledge gap, a tower-based radar has been developed for measuring temporal variation of radar signatures in a boreal forest site in southern Sweden. The instrument allows monitoring of radar signatures from the forest site over timescales ranging from less than a second to years. The experiment consists of a 50-m high tower equipped with 30 antennas, allowing fully-polarimetric tomographic imaging at microwave frequencies of P-band (420 - 450 MHz), L-band (1240 - 1375 MHz) and C-band (5250 - 5570 MHz). Results from an on-site weather station assists in interpretation of the radar results. The work in this thesis involves the design and implementation of the experimental setup and analysis of the first results. The results have provided new information about variations in forest radar backscatter during freeze-thaw cycles at P- and L-band, causing drops in backscatter of 4 to 10 dB. An effect where strong winds cause a drop in co-polarised backscatter at P-band has been directly observed for the first time. Finally, the tomographic capabilities of the instrument were demonstrated. Tomographic imaging quality was shown to be better than for measurement protocols used by previous tower-based radars when acquired while the trees were moving due to wind.

The results of this experiment are important for understanding and modelling temporal variations in radar measurements over boreal forests such that these unwanted variations can be compensated for in forest parameter estimation algorithms using SAR data.

Keywords: Synthetic aperture radar (SAR), remote sensing, tomography, temporal coherence, temporal variation, antenna array.



## ACKNOWLEDGEMENTS

The work behind this thesis was supervised by Lars Ulander, who initiated the BorealScat campaign and has trusted me with with the responsibilities involved. The initiation of the project was also greatly supported by the work of Maciej Soja and Leif Eriksson. Others at Chalmers University of Technology who have positively contributed to the work presented in this thesis are Erik Blomberg, Gunnar Elgered, Donal Murtagh, Lars Wennerbäck, Wiebke Aldenhoff, Joachim Strandberg and Alexander Vladimir Conde Jacobo.

This work was financially supported by the Hildur and Sven Winqvist Foundation for Forest Research, the European Space Agency (ESA) and the Swedish National Space Board (SNSB). Ground measurements of the site were carried out by colleagues from the Swedish University of Agricultural Sciences (SLU). Trihedral corner reflectors were installed by colleagues from the Swedish Defence Research Agency (FOI). We are also very grateful for the work done by the personnel from Mast- och tornunderhåll AB, who constructed the tower and installed the antenna array, cables, lightning protection and cameras to our demanding specifications. Thanks also to Vallebygdens Elektriska AB for their support on site when technical problems arose.

Finally, I would not be able to have done this work without the hard work of my parents, who supported me during my education.



## APPENDED PUBLICATIONS

This thesis is based on the work in the following appended Publications:

- A. A. R. Monteith, L. M. H. Ulander and M. J. Soja (2017). "Design and implementation of the BorealScat radar instrument". Department of Space, Earth and Environment, Chalmers University of Technology.
- B. L. M. H. Ulander, A. R. Monteith, M. J. Soja and L. E. B. Eriksson (2018). "Multi-port vector network analyzer radar for tomographic forest scattering measurements". Manuscript prepared for *IEEE Geoscience and Remote Sensing Letters*.
- C. A. R. Monteith and L. M. H. Ulander (2017). "Temporal survey of P- and L-band polarimetric backscatter in boreal forests". *IEEE Journal of Selected Topics in Applied Earth Observations and Remote Sensing*. Under review.

## RELATED PAPERS

The author has contributed to the following papers that are related to the work in this thesis, but are not appended in this thesis:

- I. L. M. H. Ulander, M. J. Soja, A. R. Monteith, L. E. B. Eriksson and J. E. S. Fransson (2016). “BorealScat: A tower experiment for understanding temporal changes in P- and L-band backscattering from a boreal forest”. European Space Agency, (*Special Publication*) ESA SP-740.
- II. A. R. Monteith, M. J. Soja, L. M. H. Ulander and L. E. B. Eriksson (2016). “BorealScat: A tower-based tomographic and polarimetric radar experiment in the boreal forest at P-, L- and C-band”. *International Geoscience and Remote Sensing Symposium (IGARSS)*, Beijing, China, 10-15 July 2016, pp. 7458-7461.
- III. L. M. H. Ulander and A. R. Monteith (2017). “Time series of P- and L-band forest backscatter from BorealScat”. *International Geoscience and Remote Sensing Symposium (IGARSS)*, Fort Worth, USA, 23-28 July 2017, pp. 4310 - 4313.

# CONTENTS

<b>Abstract</b>	<b>i</b>
<b>Acknowledgements</b>	<b>iii</b>
<b>Appended Publications</b>	<b>v</b>
<b>Related Papers</b>	<b>vi</b>
<b>Contents</b>	<b>vii</b>
<b>1 Introduction</b>	<b>1</b>
1.1 The Value of Forests . . . . .	1
1.2 Boreal Forests . . . . .	1
1.3 Radar Remote Sensing of Forests . . . . .	2
1.4 Relating SAR Images to Forest Properties . . . . .	4
1.5 Temporal Variation in Forests . . . . .	7
1.6 Objectives of this Thesis . . . . .	9
<b>2 State of the Art</b>	<b>11</b>
2.1 Spaceborne Synthetic Aperture Radar . . . . .	11
2.2 Airborne Synthetic Aperture Radar . . . . .	12
2.3 Tower-based Radar Remote Sensing of Forests . . . . .	12
<b>3 The BorealScat Instrument and Campaign</b>	<b>13</b>
3.1 Campaign Goals . . . . .	13
3.2 Experiment Overview . . . . .	13
3.3 The Test Site . . . . .	14
3.4 Vector Network Analyser Radar . . . . .	15
3.5 Calibration . . . . .	17
3.6 Analysis Methods . . . . .	20
<b>4 Summary of Appended Papers</b>	<b>23</b>
4.1 Paper A: Design and Implementation of the BorealScat Radar Instrument . . . . .	23
4.2 Paper B: Multi-port Vector Network Analyzer Radar for Tomographic Forest Scatter- ing Measurements . . . . .	23
4.3 Paper C: Temporal Survey of P- and L-band Polarimetric Backscatter in Boreal Forests	23
<b>5 Conclusions and Future Work</b>	<b>25</b>
<b>References</b>	<b>27</b>



# Introduction

## 1.1 The Value of Forests

Forests are to land what coral reefs are to the oceans: an expression of life in its most magnificently complex form. From a more rational perspective, forests provide habitats for other living organisms, they form the backbone of many ecosystems and unmanaged forests are among the most biodiverse places on land (Chirici, Winter, and McRoberts 2011). But more importantly and regarding Earth's ongoing climate change, forests play an important role in the Earth's carbon cycle.

Forests act as both a carbon source, whereby carbon is released into the atmosphere, and a carbon sink, whereby carbon is absorbed from the atmosphere. Carbon is released from forests through respiration, decomposition of organic matter and anthropogenic land use such as using wood for combustion. Forest trees remove carbon from the atmosphere through photosynthesis, forming the majority of the dry forest biomass as trees grow. This global terrestrial carbon flux is the largest uncertainty in our current understanding of the Earth's carbon cycle, as opposed to carbon fluxes related to fossil fuels, industry and oceans, which can be measured with relative ease (Le Quéré et al. 2016). This uncertainty results in insufficiently accurate forecasts of global warming, which may be perceived by some policy makers as unconvincing evidence to motivate the necessary regulation of anthropogenic release of carbon dioxide into the atmosphere.

This motivates the development of accurate, non-destructive measurement techniques for estimating forest properties such as tree height, tree density, stem volume and most importantly, above-ground biomass, on a global scale (Houghton, Hall, and Goetz 2009; GCOS 2016). Such measurement techniques will not only be useful for filling our knowledge gap in the Earth's carbon cycle, they will also be useful to assess storm damage, detect illegal deforestation and allow better regulation of forest use (UN-REDD 2011).

But forests should not only be viewed as instruments in order to motivate the development of better forest parameter measurement techniques. Forests have intrinsic cultural and aesthetic value. No human wants to live in a world without forests.

## 1.2 Boreal Forests

The work in this thesis specifically regards to boreal forests. Boreal forests make up the world's largest land biome and are found at latitudes of approximately 40°N to 70°N. They are characterised by conifers such as spruce, pine, fir and larch which are specifically adapted for the cold climates found at these latitudes. For example, conifers are resistant to freezing or freeze in a manner such that the trees do not experience severe permanent damage. Conifer needles have a reduced surface area and thick waxy cuticle, preventing water loss and preventing snow and ice

from sticking to them (Pielou 1988). The trees in boreal forests are also characterised by straight, vertical stems and drooping branches that facilitate the shedding of snow (Mauseth 2012).

Regarding above-ground biomass, boreal forests make up the world's second-largest terrestrial carbon stock after tropical forests. Until the last decade, boreal forests have been viewed as a carbon sink, but recent studies indicate that this carbon sink may be turning into a carbon source, mainly due to rising temperatures in the boreal zone (Stephens et al. 2007; Pan et al. 2011). A continuation of this trend will result in more frequent forest fires, insect outbreaks, permafrost loss and accelerated climate change (Bradshaw and Warkentin 2015). But due to inadequate biomass estimation methods, a high uncertainty is associated with these claims (Shvidenko et al. 2010; Bradshaw, Warkentin, and Sodhi 2009). It is therefore important to map the above-ground biomass density of boreal forests and also to do so repetitively over time in order to monitor changes in land use, natural degradation and carbon flux.

### 1.3 Radar Remote Sensing of Forests

The most accurate method for above-ground forest biomass estimation is to cut down trees and weigh the mass of the stems, branches and leaves or needles. This is obviously too destructive to apply on a global scale, so non-invasive methods are needed. A sample of trees must however be cut down and weighed to develop allometric equations relating the weighed above-ground biomass to tree properties such as stem diameter, canopy height, basal area, crown volume and wood density for a given species (Van Laar and Alparslan 2007; Petersson 1999; Marklund 1988). Such allometric relationships facilitate non-destructive biomass estimation by instead making measurements of the forest structure of a sample of trees, often within a 10-meter radius forest plot, which is then extrapolated to stand-level<sup>1</sup>. While this measurement method results in accurate estimates of forest parameters it is not feasible to apply on a global scale if based on *in-situ* field measurements, calling for remote sensing methods.

Small-footprint airborne lidar can be used to make accurate measurements of the forest structure, from which biomass estimates can be calculated (Nelson, Krabill, and MacLean 1984; Drake et al. 2002). But due to the cost of flight time, sparse sampling of lidar measurements and the significant amount of field data needed for calibration, this method is too expensive to apply on a global scale (Hyde et al. 2007). Spaceborne lidar has the potential of providing global coverage, but suffers from sparse coverage in time and space. One such example is the future Global Ecosystem Dynamics Investigation (GEDI) spaceborne lidar mission (NASA 2015). Coverage by GEDI will be limited to latitudes within  $\pm 52^\circ\text{N}$ , which is mostly below the boreal zone, because the International Space Station will be used as a platform. Lidar signals are also not capable of penetrating clouds, which are often present over tropical and boreal forests.

Radar signals are capable of overcoming many of these limitations. Radars using electromagnetic waves in the lower microwave region (300 MHz to 30 GHz) are capable of penetrating clouds, giving better temporal coverage of forests. The lower limit of 300 MHz is imposed by severe distortions caused by the ionosphere in the spaceborne radar case (Shteinshleiger et al. 1997). Better spatial coverage is obtained by wide antenna radiation beams, capable of covering a large area on the Earth's surface. Electromagnetic waves with frequencies up to approximately

---

<sup>1</sup> Forests, especially productive forests, are often delineated into stands, which are areas of trees which are homogeneous in terms of density, age, species etc.

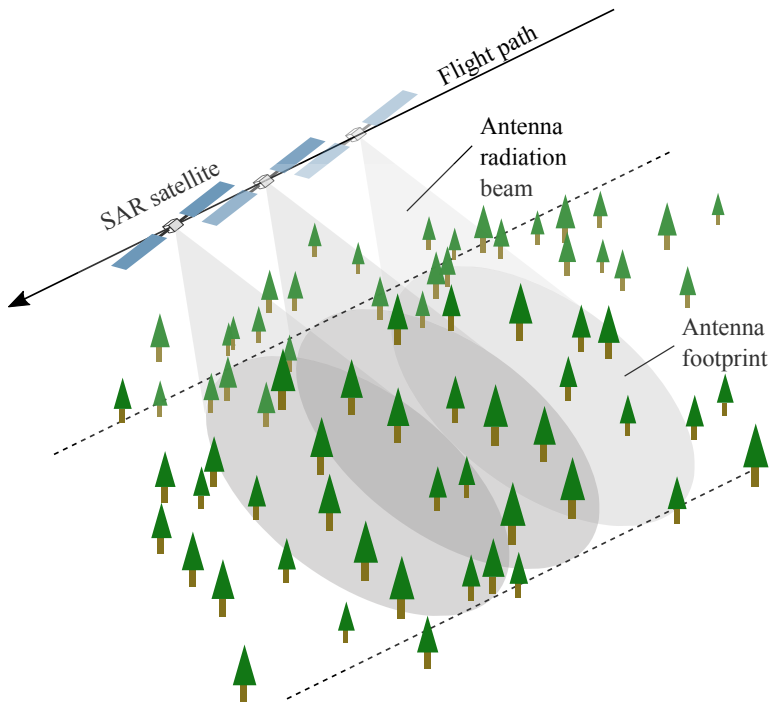


Figure 1.1. *Illustration of how spaceborne SAR measurements are acquired over a forest. Each instance of the satellite and associated radiation beams represent a pulse that is transmitted and received as the satellite orbits the Earth. Several such pulses are combined through signal processing to form an image of the surface reflectivity, from which forest parameters can be estimated.*

2 GHz are capable of penetrating the forest canopy and reflecting off larger structures such as the stems and large branches, which contain the majority of the above-ground biomass. The electromagnetic field scattered from a forest scene that is sensed by the radar can therefore be used to estimate the above-ground biomass (Wu 1987; Le Toan et al. 1992; Hussin, Reich, and Hoffer 1991; Dobson et al. 1992; Ranson and S. 1994).

The radar signal frequency determines the size of the antenna aperture necessary to emit an electromagnetic wave at such a frequency, where lower frequencies require larger antenna apertures. The aperture size in turn determines the spatial resolution at which the biomass can be mapped, where larger apertures provide finer spatial resolution. A spatial resolution on the order of tens of meters is necessary for reducing the variance in biomass density estimates and to separate the scattered field from the forest from contributions of other structures such as buildings, fields and water bodies. An antenna in Earth's orbit capable of providing such a fine resolution at microwave frequencies suitable for biomass estimation would be impractically large for launching into orbit, motivating the use of a synthetic aperture radar (SAR) (Cumming and Wong 2006).

A SAR allows the use of a smaller antenna, which is feasible to launch into Earth's orbit, while still providing the necessary resolution for biomass mapping. A SAR achieves this by sending and

receiving multiple electromagnetic pulses as the platform, e.g. an aeroplane or satellite, travels above the Earth's surface (see Figure 1.1). Several pulses are then combined through signal processing algorithms to form an image of the surface reflectivity. The spatial resolution of these images is then the same as would be achieved had the antenna aperture been twice as large as the distance travelled by the SAR over which the pulses used in image reconstruction were collected. Our task is to convert these SAR images to accurate maps of forest properties, e.g. biomass density per unit area, by developing suitable parameter estimation algorithms. This requires a good understanding of how SAR images are related to forest properties.

## 1.4 Relating SAR Images to Forest Properties

The signal measured by a SAR consists of electromagnetic fields scattered from the forest below. The choice of radar system parameters and processing methods give different information about the forest, providing a variety of SAR observables that can be used in forest parameter estimation algorithms.

### Backscatter

The power echoed from an object can be related to the object's *radar cross-section*  $\sigma$  through the radar equation. For a monostatic radar with atmospheric and internal losses neglected, the radar equation is

$$P_r = P_t \frac{G^2 \lambda^2}{(4\pi)^3 R^4} \sigma \quad (1.1)$$

where  $P_r$  is the received power,  $P_t$  is the transmitted power,  $G$  is the antenna gain,  $\lambda$  is the wavelength and  $R$  is the radar-object distance. The radar cross-section of a point target is defined as

$$\sigma = \lim_{R \rightarrow \infty} 4\pi R^2 \frac{|E^s|^2}{|E^i|^2} \quad (1.2)$$

where  $E^s$  is the scattered electric field amplitude and  $E^i$  is the incident field amplitude. But forest consists of many complicated structures resulting in randomly distributed scatterers. For two-dimensional SAR images it is therefore useful to define the *backscattering coefficient*  $\sigma^0 = \langle \sigma \rangle / A$ , which is the average radar cross-section per unit area  $A$ . An approach to relating SAR images to forest properties, e.g. biomass, is to model these properties in terms of the backscattering coefficient  $\sigma^0$ .

### Choice of radar frequency

The choice of radar frequency determines which structures within the forest will contribute to the backscatter. This concept is illustrated by Figure 1.2, showing the radar cross-section for perfect electrically conducting spheres of different sizes at different radar frequencies. The figure illustrates that smaller objects (e.g. leaves and needles) scatter microwave radiation at higher frequencies, while lower frequency waves pass through these scatterers. But larger objects (e.g. tree trunks and large branches) do scatter lower-frequency microwave radiation.

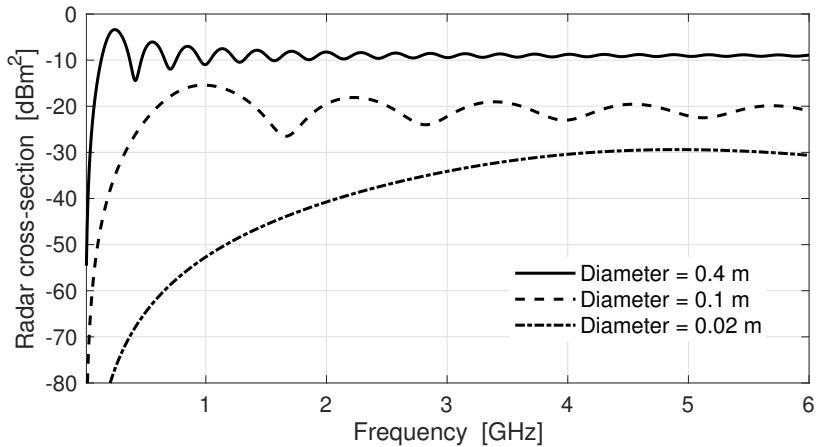


Figure 1.2. *Monostatic radar cross-section of a perfect electrically conducting sphere as function of sphere diameter and radar frequency. The plot shows that smaller scatterers (smaller spheres) result in a lower backscatter at lower radar frequencies compared to higher frequencies. Radars operating at lower frequencies (e.g. P-band) can therefore be used to observe branches and trunks below a forest canopy, whereas higher-frequency waves (e.g. X-band) cannot penetrate the canopy.*

At higher frequencies such as X-band (8 - 12 GHz) and C-band (4 - 8 GHz), the scattering centre is at the upper canopy of the forest since shorter wavelengths of electromagnetic radiation are increasingly scattered and attenuated by smaller structures than longer wavelengths. At L-band (1 - 2 GHz), the radar pulses travel through the canopy and reflect off branches and trunks, making SARs at L-band more suitable for biomass estimation. However, for high-biomass forests the biomass-backscatter curve saturates due to attenuation in the forest canopy, making L-band SAR images less sensitive to biomass densities above 100 t/ha. At lower frequencies such as P-band (420 - 450 MHz) (IEEE 2003) the scattered fields originate mostly from the stems, in particular the stem-ground double-bounce interaction, and direct backscatter from large branches in the canopy. This places the scattering centre close to the ground. The biomass-backscatter relationship still saturates but it does so at higher biomass densities than for L-band, making P-band SAR better for biomass estimation than L-band (Israelsson, Askne, and Sylvander 1994). To completely overcome the backscatter saturation for high biomass forests, SARs operating in the VHF band (30 - 300 MHz) can be used (Israelsson, Ulander, et al. 1997; Fransson, Walter, and Ulander 2000; Smith and Ulander 2000; Smith-Jonforsen, Ulander, and Luo 2005). But electromagnetic waves at these frequencies experience distortion introduced by the ionosphere, limiting their use to airborne SARs (Shteinshleiger et al. 1997; Belcher and Rogers 2009).

## Polarimetry

In addition to frequency, electromagnetic plane waves are also characterised by their polarisation, which specifies the direction of electric field oscillations. A fully polarimetric radar is capable of transmitting and receiving both horizontally (H, parallel to the Earth's surface) and vertically (V,

orthogonal to H and the direction of travel) polarised waves. The scattered fields in each pixel of a SAR image can then be separated into the HH, HV, VH and VV contribution, where the first letter is the receiving polarisation and the second the transmitted polarisation (Ulaby et al. 2014; Lee and Pottier 2009). The opposite of this convention is also seen in literature.

SAR polarimetry allows the decomposition of different scattering mechanisms. At P-band, co-polarised backscatter, i.e. VV and HH, is dominated by reflections from large branches and the double-bounce scattering mechanism for trees with straight, vertical trunks, such as most conifers in boreal forests. The cross-polarised backscatter, i.e. HV and VH, originates from a geometry that depolarises the incoming wave, often randomly orientated branches in the canopy<sup>2</sup>. Different polarisations have different degrees of sensitivity to biomass. In boreal forests, HV and HH backscatter have been found to show the greatest sensitivity to biomass at P-band. Current P-band biomass estimation models include a combination of backscatter terms from different polarisations. Even including VV backscatter, which shows little sensitivity to biomass on its own, has been shown to reduce the variance of biomass estimated if included in a model (Soja, Sandberg, and Ulander 2013). Finding the polarimetric composition that best separates scattering contributions is an active research topic.

## Interferometry

SAR interferometry provides information about the effective scattering height (Bamler and Hartl 1998). Larger trees with more biomass tend to have a higher scattering height, providing a SAR observable that is related to biomass and can be included in estimation models. SAR interferometry makes use of two SAR images over the same forest site, where the antenna platform views the forest at slightly different angles for the two images. The images are combined to produce the interferometric coherence magnitude and the interferometric phase. The interferometric phase is directly related to the effective scattering height, but has high variance if the coherence is low. The coherence is a measure of similarity between the complex SAR images and is determined by the acquisition geometry, thermal noise, processing algorithm and changes in the scattering characteristics of the forest between the two acquisitions, called temporal decorrelation (Zebker and Villasenor 1992; Ulaby et al. 2014).

SAR interferometry can be achieved by multiple orbital passes of the SAR satellite over the same site, known as repeat-pass SAR interferometry. A drawback of this method is that the orbital passes are separated by time intervals of hours to days, during which moisture and geometrical changes can take place in the forest, resulting in temporal decorrelation. This problem can be overcome by having two antennas on the same platform (e.g. NASA's Shuttle Radar Topography Mission) or two antenna platforms orbiting the Earth in close proximity (e.g. DLR's TanDEM-X), called single-pass interferometers. In the latter case, the acquisition time interval between the two SAR images may still be on the order of milliseconds to seconds, during which significant temporal decorrelation could occur in forests due to wind (Narayanan, Doerr, and Rundquist 1992; Billingsley 2002).

---

<sup>2</sup>HV and VH are the same in a monostatic radar configuration, which is the case for airborne and spaceborne SARs.

## **Tomography**

SAR tomography allows the separation of scatterers with different heights (Reigber and Moreira 2000). This is useful for separating the backscatter contributions at different heights, e.g. from the forest canopy and the ground, providing observables that are more closely related to above-ground biomass. This is achieved by combining multiple SAR images of the same forest site, each acquired at a different angle to the forest. The result is a three-dimensional volume of the reflectivity, assuming that the entire forest volume has been illuminated.

Several orbital passes of the SAR satellite are required to form a SAR tomogram, called repeat-pass SAR tomography. The time intervals in between these acquisitions may result in severe temporal decorrelation, reducing the quality of tomography observables. Repeat-pass SAR interferometry of forests is therefore only feasible at lower frequencies, such as at P-band or lower, where larger changes in geometry or dielectric properties of the forest are necessary to result in significant temporal decorrelation (Dinh, Tebaldini, Rocca, and Le Toan 2015). Due to its ability to penetrate forest canopies, there is also an interest in SAR tomography at L-band, although the severity of temporal decorrelation at L-band does not facilitate repeat-pass SAR tomography. Instead, the aim is to acquire an interferometric pair of SAR images at the same time using two antenna platforms orbiting in close formation, such that temporal decorrelation is negligible. Several such interferometric pairs acquired with a single-pass interferometer over multiple orbital passes are then combined through spectral estimation techniques, in particular coherence tomography, to form a SAR tomogram that is more robust to temporal decorrelation (Cloude 2006).

## **1.5 Temporal Variation in Forests**

The above-mentioned SAR observables used to estimate forest properties are dependent on the electromagnetic scattering properties of forests. These are determined by the radar system parameters, such as frequency and polarisation, the acquisition geometry, ground topography and the forest dielectric properties and structure. The dielectric properties in the forests are dominated by liquid water content, as in the soil and trees, and its temperature (Torgovnikov 1993). The forest structure contributing to SAR imagery is dependent on the signal frequency, where lower frequency waves are scattered and absorbed by forest structures larger than a tenth of a wavelength in size.

Ideally, these forest properties should only be dependent on the biomass for the development of parameter estimation models using SAR images. But natural environments such as forests are highly dynamic as they respond to environmental changes, and these changes occur at timescales ranging from a fraction of a second to years.

### **Wind**

Wind has the effect of causing geometrical changes at timescales of less than a second to several seconds. Microwaves such as at C-band or X-band are scattered by leaves, needles and small branches. Even a small amount of wind can cause large variations in the scattered field, causing significant temporal decorrelation between two SAR acquisitions even at such short timescales. Lower frequency waves are more sensitive to larger structures in forests, which are more stable

in wind. However, the double-bounce scattering mechanism, which is dominant for straight, vertical trunks, is sensitive to wind at P-band. Even a small tilt in the trunk due to wind can cause significant deviations in backscatter. This is because vertical stems above a flat ground act as retroreflectors for co-polarised radar channels (HH and VV), but not when the ground-trunk angle is even slightly off  $90^\circ$ . One can therefore expect both a drop in coherence and a drop in co-polarised backscatter during windy times for P-band.

### **Freeze-thaw cycles**

Water in liquid form has a dielectric constant of approximately 80, whereas ice has a dielectric constant close to 3 (Wolfe and Bryant 2001). This significant variation in dielectric constant should be considered in radar remote sensing of boreal forests, that commonly experience sub-zero air temperatures. Frozen soil moisture appears more transparent to microwaves, decreasing the backscatter arising from the double-bounce scattering mechanism, such as at P-band. Frozen stem and branch moisture also make the trees appear more transparent for microwaves, decreasing the backscatter at higher radar frequencies as well (Way et al. 1990; Ackermann 2015; Pulliainen, Kurvonen, and Hallikainen 1999; Rignot, Way, and Viereck 1994; Santoro, Fransson, et al. 2009). Thus the entire forest volume experiences changes in scattering characteristics during sub-zero temperatures. Normal levels of backscatter are restored as the air temperature returns above  $0^\circ\text{C}$ . These variations in backscatter during freeze-thaw cycles, which occur on timescales of hours to days, are accompanied by large variations in temporal coherence.

### **Seasonal variations**

In addition to sub-zero air temperatures during winter, boreal forests also respond to changes in the environment during the growing season, in particular the soil moisture content and vapour pressure deficit (VPD). VPD is the difference between the partial pressure of water vapour in the air and in the leaf, and is the driving force of transpiration. A moderate VPD results in healthy transpiration, where the plant moisture lost to evaporation is replaced by the uptake of moisture available in the soil, maintaining a constant stem moisture content and thus dielectric constant (McDonald, Zimmermann, and Kimball 2002).

This equilibrium is disturbed in the winter when the soil is frozen but the VPD is high enough for transpiration to take place in evergreen conifers, such that water uptake by the roots is not possible. The stem moisture content, and thus dielectric constant, then fluctuates with temperature. The equilibrium is also disturbed in summer during very warm, dry conditions resulting in a very high VPD and low soil moisture content. In this case the stem moisture lost to evaporation cannot be replaced by water uptake from the soil, resulting in a net decrease in water stem water content until rainfall increases the soil moisture content (Sparks, Campbell, and Black 2001). However, conifers do have some capability of limiting evaporation through closing and opening of their stomata. These mechanisms result in backscatter variations on timescales of days to weeks.

### **Why study temporal variation?**

The previous sections have highlighted how SAR observables used for forest parameter estimation can be affected by environmental variations. If unaccounted for, these variations increase the variance of forest parameter estimates, and can result in biased estimates (Sandberg, Ulander,

Wallerman, et al. 2014; Sandberg, Ulander, Fransson, et al. 2011; Soja, Sandberg, and Ulander 2013; Saatchi et al. 2007; Santoro, Eriksson, and Fransson 2015). While estimation variance can be reduced by spatial averaging, biased estimates cannot be corrected no matter the sample size. Wind, freeze-thaw cycles and seasonal variations cause biases in backscatter and lower the temporal coherence. This calls for a very good understanding and modelling of temporal variations of radar signatures over boreal forests and the contributing scattering mechanisms in order to be able to compensate for these unwanted variations in forest parameter estimation models.

## **1.6 Objectives of this Thesis**

The objectives of the work in this thesis are to lay the foundation of the BorealScat experiment, demonstrate its capabilities and analyse the first results. The purpose of this experiment is to study the temporal decorrelation and influence of seasonal and weather effects on polarimetric radar measurements over a site representative of boreal forests at P-, L- and C- bands throughout the vertical structure of the forest. The results from the BorealScat experiment provides valuable information about the electromagnetic scattering mechanisms and temporal variations in boreal forests, which will help in modelling these behaviours in forest parameter estimation models.

The following chapters and appended publications detail the design and implementation of the BorealScat experiment, show results from backscatter and coherence time series analyses and demonstrate the first tomographic reconstructions from experimental data.



## State of the Art

### 2.1 Spaceborne Synthetic Aperture Radar

The lowest-frequency civilian SAR currently in Earth's orbit is JAXA's ALOS-2 satellite. The PALSAR-2 SAR is quad-polarised (HH, HV, VH and VV), although only dual-polarised acquisitions (HH and HV) are acquired over the boreal regions with 2 to 6 acquisitions per year (JAXA 2017). Due to the sensitivity of L-band radar signatures to temporal variations in forests, this mission is not suitable for SAR interferometry or SAR tomography over forests. A possible future mission, Tandem-L by the German Aerospace Center DLR, will feature two SARs flying in formation such that an interferometric pair can be acquired within a time interval on the order of seconds, allowing for SAR interferometry and SAR coherence tomography (Moreira et al. 2015). Thus only short-term temporal decorrelation will affect forest parameter estimates.

Forest monitoring at C-band is also of high interest, which is driven by the available SAR data from ESA's Sentinel-1 satellites (Torres et al. 2012; Torres et al. 2017). This dual-polarised SAR mission currently consists of two identical satellites (Sentinel 1A and 1B) in Earth's orbit but 180° out of phase, offering a 6-day repeat cycle. The high temporal decorrelation over this timescale at C-band over forests makes this mission of limited use for SAR interferometry and tomography over forests. A proposed mission concept is therefore to add a companion satellite to one of the existing Sentinel-1 satellites to allow the acquisition of interferometric pairs with little temporal decorrelation (Regan, Silvestrin, and Fernandez 2016; Sephton and Wishart 2013; Rott et al. 2017).

One tandem mission is already in orbit, i.e. DLR's TanDEM-X mission, consisting of two quad-polarised X-band SAR sensors orbiting in close formation (Krieger et al. 2007). The interferometric pairs acquired during tight formation flying over forests have essentially no temporal decorrelation. These SAR observables have been shown to be useful for estimating forest biomass in boreal forests assuming a known digital terrain model and suitable allometric equations (Askne, Fransson, et al. 2013; Soja, Persson, and Ulander 2015; Askne, Soja, and Ulander 2017).

With regards to radar remote sensing of forests, a SAR operating at a frequency capable of better forest volume penetration than L-band is needed. This will allow for backscatter saturation at higher values of forest biomass and better illumination of the forest volume for SAR tomography. This need will be fulfilled by ESA's BIOMASS mission which was selected to be ESA's seventh Earth Explorer in 2013 (ESA 2012). This single satellite will feature a quad-polarised SAR and will be the first spaceborne P-band SAR. The satellite will operate in a repeat-pass SAR tomography mode for the first nine months, providing vertical distributions of forest backscatter. Tomograms will be reconstructed from seven acquisitions, each separated by three days. High temporal coherence on the order of days to months is therefore desirable at P-band. The launch for BIOMASS is planned for the year 2021.

## 2.2 Airborne Synthetic Aperture Radar

In airborne SAR campaigns, SAR images are acquired over a site using SARs mounted on aeroplanes. Such campaigns are useful for evaluating new spaceborne SAR concepts and for the development of forest parameter estimation algorithms when the existing SAR satellites do not feature the capabilities of interest.

In boreal forests, the BioSAR campaigns (2007, 2008 and 2010) have provided valuable fully polarimetric L- and P-band SAR data for developing biomass estimation algorithms, performing the first SAR tomography analysis in boreal forests and studying temporal changes in boreal forests (Hajnsek et al. 2008; Hajnsek et al. 2010; Ulander et al. 2011). Two boreal-like forest sites in Sweden were imaged: the Krycklan river catchment ( $64^{\circ} 14' N$ ,  $19^{\circ} 46' E$ ) in northern Sweden and the Remningstorp experimental forest site ( $58^{\circ} 28' N$ ,  $13^{\circ} 38' E$ ) in Southern Sweden. Temporal coherence was a key interest in the BioSAR campaigns, but it could only be studied on timescales of one to two months and three years. Furthermore, only a few temporal samples were acquired. Coherence at P-band was found to remain high during one month whereas L-band coherence was lower for such timescales. HH-polarisation was found to exhibit the highest coherence, which was attributed to the stable double-bounce mechanism, whereas HV-polarisation showed the lowest coherence. The causes of temporal decorrelation were not examined.

## 2.3 Tower-based Radar Remote Sensing of Forests

In order to study the temporal variation of SAR observables in tropical forests, the TropiScat campaign was initiated in French Guiana (Albinet, Borderies, Kolečk, et al. 2012). The experiment consisted of a 55-m high tower equipped with an antenna array capable of acquiring quad-polarimetric radar data over a tropical forest site at P- and L- band. The antenna array allowed tomographic analyses of the forest site over time (Dinh, Tebaldini, Rocca, Kolečk, et al. 2013). Data was acquired at intervals of 15 minutes for more than a year. Data from on-site meteorological and soil moisture sensors allowed an analysis of how SAR observables are affected by environmental variations in tropical forests. This experiment provided valuable information about the temporal coherence at different timescales, diurnal variations in backscatter, changes in the effective scattering height with time and what scattering mechanisms are involved. It also provided the optimal times of the day (6:00 and 18:00) for acquisitions by the future BIOMASS satellite such that the effects of environmental parameters on SAR observables are minimised (Borderies et al. 2013). In 2015 this study was extended with a second tower-based radar, AfriScat, in the tropical forests of Ghana (Albinet, Kolečk, et al. 2015). A similar, but smaller-scale experiment where a single temperate tree in France was studied showed that the backscatter and temporal coherence was very sensitive to temperature and moisture conditions (Albinet, Borderies, Floury, et al. 2016). This suggested dependence of SAR observables on the dielectric constant of the soil, tree trunk and transpiration mechanisms.

The results from these experiments cannot be extrapolated to boreal forests due to significant differences in climate and forest structure between the biomes. No experiment studying the temporal variation of SAR observables over timescales of minutes to years has been done before in boreal forests. To fill this knowledge gap, the BorealScat tower-based radar campaign was initiated by Chalmers University of Technology (Ulander et al. 2016).

# The BorealScat Instrument and Campaign

## 3.1 Campaign Goals

The goal of the BorealScat campaign is to study the temporal decorrelation and influence of seasonal and weather effects on polarimetric radar measurements over a boreal forest at P-, L- and C-band throughout vertical structure of the forest. It is expected that the results will also reveal information about the electromagnetic scattering mechanisms taking place in boreal forests during SAR acquisitions. This information will then be incorporated into forest parameter estimation models using SAR data to increase the accuracy of the estimates.

## 3.2 Experiment Overview

The experiment consists of a tower-based research station in the Remningstorp experimental forest site in southern Sweden ( $57^{\circ} 27' 5''$  E,  $13^{\circ} 37' 35''$  N). Figure 3.1 illustrates the layout of the experiment site. An array of antennas is situated at the top of the tower and is connected to a multi-port vector network analyzer (VNA) in an equipment hut at the base of the tower via low-loss cables. The VNA generates the microwave signals which are emitted as electromagnetic waves by one of the antennas on the tower. The field scatters off the forest near the tower and is received by the array of antennas on the tower. These signals from the antennas are sampled in parallel by the multi-port VNA.

The purpose of the antenna array is to allow tomographic radar imaging of the forest below at HH, HV, VH and VV polarisation. The physical configuration of antennas in the array and the frequency at which they operate determine the spatial resolution and height of ambiguity of the reconstructed tomographic image. A fine resolution and large height of ambiguity are desired for producing accurate, unambiguous vertical profiles of forest backscatter. But for a given number of antennas, the antenna configuration design is a trade-off between resolution and height of ambiguity. To achieve accurate, unambiguous tomographic imaging at P-, L- and C-band, two antenna arrays were designed and implemented: one optimised for P- to L-band and the other optimised for C-band.

Unlike the TropiScat and AfriScat campaigns, a multi-port VNA is used, allowing parallel measurements of the scattered fields sensed by all antennas for a given frequency band. This is opposed to using a two-port VNA where the signals are routed to the antennas via an array of slow, failure-prone mechanical switches. These fast measurements allow for tomographic imaging which is more robust to short-term temporal decorrelation due to wind.

Fully-polarimetric tomographic measurements are acquired from P- to C-band every 5 minutes and it is planned to continue to do so for 3 years. To support the analysis of the radar observables, an on-site weather station collects local meteorological and soil moisture data.

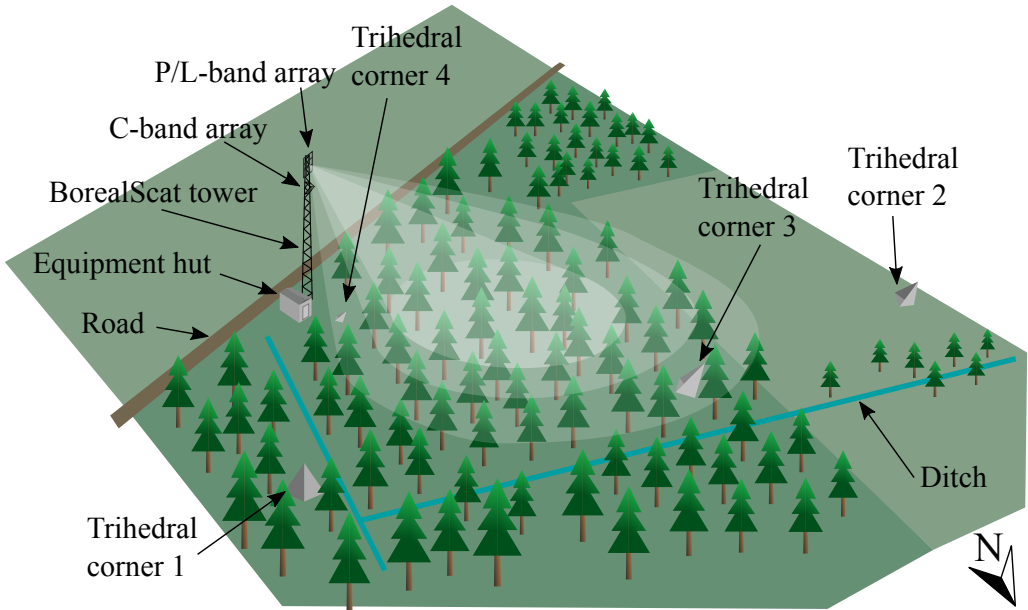


Figure 3.1. Illustration of the BorealScat experiment site. The illuminated region corresponds to the P/L-band region of illumination. The C-band region of illumination is not shown. Trihedral corner reflectors 1 to 3 have short sides of 5.1 m whereas trihedral corner reflector 4 has a short side of 70 cm. Reflector 3 is concealed in the forest, whereas the others all are in direct line of sight of the antennas.

### 3.3 The Test Site

The forest stand under observation in this experiment consists mainly of mature Norway Spruce (*Picea abies* (L.) Karst.). Tree heights in the stand vary from approximately 25 m to 27 m with an above-ground biomass density of 250 tons/ha as estimated in the fall of 2014 from ground inventory measurements. Figure 3.2 shows the forest as viewed from surveillance cameras on the tower. The topography is relatively flat, which along with the stems of the trees results in a strong double-bounce backscattering contribution at longer wavelengths. During winter the site is exposed to sub-zero temperatures and snow, with soil moisture remaining high during most of the year. These features make the site representative of boreal forests.

The site was also selected based on ease of access by car, electricity supply and suitable places for placing trihedral corner reflectors for calibration.



Figure 3.2. *The forest under observation as viewed from the tower at a height of 20 m (left) during winter and 37 m (right) during autumn.*

### 3.4 Vector Network Analyser Radar

Airborne and spaceborne SARs most commonly use chirp waveforms as the transmitted signal, where the carrier frequency is modulated such that the signal frequency is continuously swept across the desired bandwidth (Richards, Scheer, and Holm 2010). This waveform is suitable in situations where very fast and wideband measurements must be made, the antenna-scene distance is large, the radar must be Doppler tolerant and high average transmitted power is necessary, as is the case with most airborne and spaceborne SARs. For the BorealScat instrument, such fast measurements (on the order of millisecond intervals) are not necessary and the radar must operate across a very wide frequency range (P-band to C-band). Wide instantaneous receiving bandwidths of radars are wide doorways for noise, decreasing the dynamic range. This means that weak scatterers, such as branches cannot be detected. This poor dynamic range could be increased by increasing the transmit power of the radar, but wideband power amplifiers are difficult to design due to nonlinear input-output responses.

The solution is to do very narrow-band measurements, one at a time, each time stepping to a different frequency until the desired bandwidth is covered. On the receiving end, the received signal is passed through a narrow bandpass filter to filter out wideband noise. The resulting measurement has a very wide dynamic range. This is known as a stepped-frequency continuous wave (SFCW) radar (Richards 2014), and VNAs are off-the-shelf instruments capable of carrying out such a measurement.

#### Raw data

To cover a frequency band, the VNA transmits and receives a gated continuous wave starting at the lowest frequency  $f_{start}$  and stepping at a constant frequency step of  $\Delta f$  until it reaches the highest frequency  $f_{stop}$ . The bandwidth covered is  $B = f_{stop} - f_{start}$  with centre frequency  $f_c = (f_{start} + f_{stop})/2$  and the number of frequency points covered in the band is  $K = B/\Delta f + 1$ . This transmitted signal is illustrated in Figure 3.3.

At each frequency step the VNA produces a complex number, known as S-parameters. The magnitude of S-parameters is the amplitude of the received continuous wave divided by the

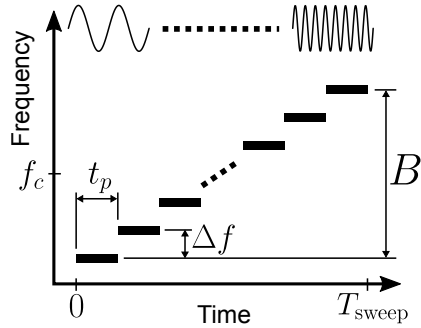


Figure 3.3. Plot of an SFCW waveform that is emitted by a VNA. Several monochromatic pulses with duration  $t_p$  are emitted in sequence with increasing frequencies (steps of  $\Delta f$ ) to cover a bandwidth  $B$ . The duration of the frequency sweep is  $T_{\text{sweep}}$ . The centre frequency of the sweep is  $f_c$ .

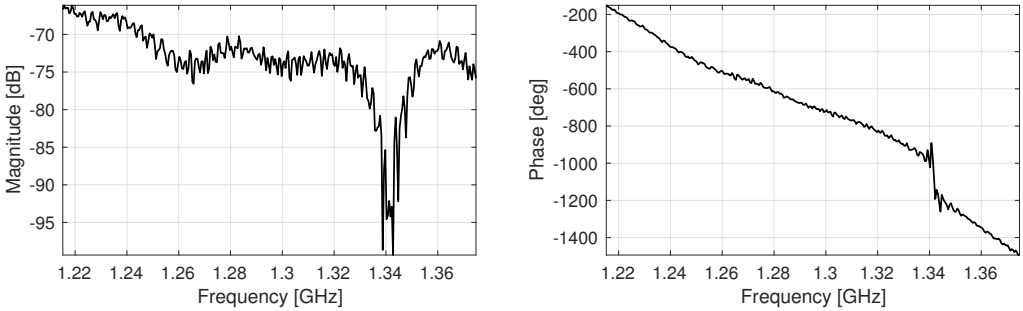


Figure 3.4. Plots of the raw VNA data with phase calibration of one frequency sweep consisting of a magnitude plot (left) and phase plot (right). This measurement was carried out at L-band, HH-polarisation. Inferring information about the forest scene from the data in this form is difficult, if not impossible due to strong mutual coupling between antennas.

amplitude of the transmitted continuous wave. This magnitude is therefore a function of losses in cables, the antenna gain patterns, connector insertion loss, free-space path loss, and backscatter from the forest scene. The phase of S-parameters is the phase shift between the transmitted and received continuous waves, which is a function of propagation delays in cables, propagation time in air and phase shifts caused by scatterers in the forest scene. From a traditional radar point of view, the S-parameter vector measured by a VNA radar is equivalent to the frequency-domain representation of a repetitive chirp signal, swept across the bandwidth  $B$ , after matched filtering, assuming a perfectly stable scene.

Figure 3.4 shows an example of an L-band, HH-polarised VNA radar measurement. Inferring information about the scene directly from these plots is difficult, if not impossible. In fact, these results are dominated by mutual coupling between the transmitting and receiving antennas, not the fields scattered from the forest. We therefore want to separate the radar returns originating from different ranges from the antennas by transforming the raw data into range profiles.

## Range profiles

A range profile (scattered power density as a function of range) is created from S-parameters by inverse Fourier transformation. Since the S-parameters are discrete-time signals, this is done by the inverse discrete Fourier transform (iDFT). Artefacts called sidelobes exist in such range profiles due to the finite bandwidth  $B$  of the frequency-domain signal measured by the VNA and have the undesired effect of spreading scattered power originating from one range to other ranges. Such sidelobes in range can be suppressed by applying a tapering window function on the S-parameters before inverse Fourier transformation. A range profile can be expressed as

$$s_{ij}(n) = \text{iDFT} \{S_{ij}(k)W_R(k)\} \quad (3.1)$$

where  $S_{ij}(k)$  is the S-parameter vector measured by the VNA for transmitting antenna  $j$  and receiving antenna  $i$ . The frequency point index in the band is denoted  $k = 1, 2, \dots, K$  such that the frequency  $f(k) = f_{start} + (k - 1)\Delta f$ .  $W_R(k)$  is the window function for sidelobe suppression in range, which in this thesis was chosen to be the Hamming window (Rawat 2015). The length of the iDFT operation determines range sampling interval  $\Delta R$  and implicit time-domain sampling rate  $f_s$ . For a complex signal, the Nyquist criterion is satisfied if  $f_s \geq B$ . The iDFT length is then  $N = f_s/\Delta f + 1$ , giving a range interval of  $\Delta R = c_0/(2f_s)$ , where  $c_0$  is the speed of light in a vacuum. The range index is denoted  $n = 1, 2, \dots, N$  such that the one-way range from the antennas  $R(n) = (n - 1)\Delta R$ . Due to the periodicity assumption of the iDFT, a maximum possible range of unambiguous observation for a VNA radar exists which is  $R_u = c_0/(2\Delta f)$ . Figure 3.5 shows an example of a range profile from an L-band SFCW measurement and how it can be related to the acquisition geometry. The range profile can be corrected for free-space path loss as

$$r_{ij}(n) = R^2(n)s_{ij}(n) \quad (3.2)$$

## 3.5 Calibration

The range profile  $r_{ij}(n)$  is complex valued and requires calibration of the magnitude and phase before information about forest scattering can be inferred. The work in this thesis only concerns variations in forest backscatter over time, not absolute values of backscatter. This requires a relative calibration, where temporal variations in the received signals due to variations in the impulse response of components in the radar system are compensated for. The resulting variations in radar measurements over time can therefore be attributed to variations in the forest only.

### Reference cable

To compensate for unwanted temporal variations in the internal characteristics of the VNA, the ports of the VNA are first connected to a series of mechanical switches capable of routing any of the transmit and receive ports via a single reference cable. The switches and reference cable are housed within the temperature-controlled hut and are therefore assumed to have a constant impulse response over time. Variations in the impulse response of the reference cable then indicate variations in the VNA measurement characteristics and can be compensated for using the ratio method of relative calibration (Ulaby et al. 2014).

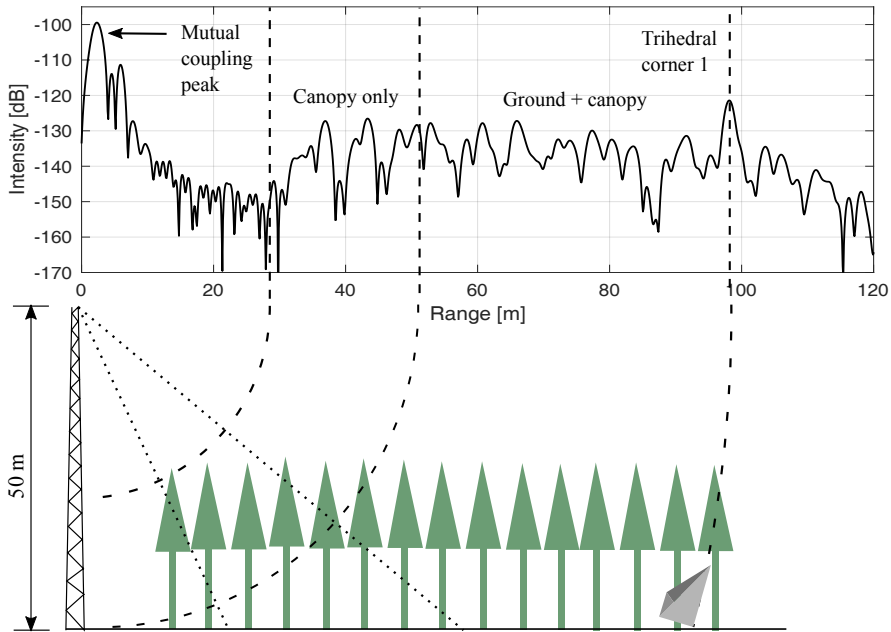


Figure 3.5. Magnitude squared of an HH, L-band range profile before compensation for free space loss ( $s_{ij}(n)$ ) with an illustration of how the curve relates to a two-dimensional slice in the acquisition geometry. The dotted lines indicate the interval of incidence angle at ground level relevant to spaceborne SAR missions.

### Direct coupling peak

To compensate for unwanted temporal variations in propagation loss of the cables leading up the tower to the antennas, a reference beyond the cable ends are needed. Significant mutual coupling between antennas in the P- to L-band antenna array occurs. This forms a peak at the start of the range profile (see Figure 3.5), which should be constant with time since it depends only on the components at the top of the tower. The ratio method of relative calibration can then be used to normalise for variations in this peak. Unfortunately, rainfall results in wet antenna radomes, which disturb the antenna patterns. This relative calibration can therefore not be applied during rainfall events. An example of this direct coupling as it varies with time for L-band, HH-polarisation is shown in Figure 3.6.

### Trihedral corner reflectors

Trihedral corner reflectors act as strong, stable point scatterers in the observed scene. If the exact distance between an antenna and the apex of a trihedral corner reflector is known, systematic phase errors in the range profile, from for example cable propagation delays, can be compensated for. However this is only possible when the backscatter from the corner reflector is strong enough that it can be separated from the backscatter contribution of the surrounding clutter (Ulaby et al.

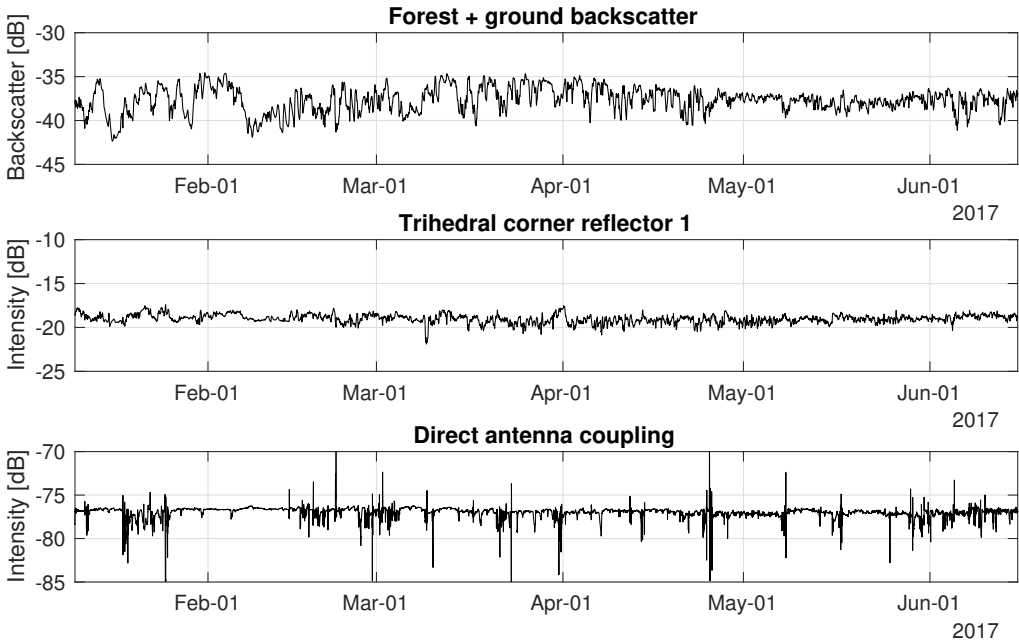


Figure 3.6. *Time series of the forest backscatter trend, trihedral corner reflector response intensity trend and direct antenna coupling intensity for L-band HH-polarisation over a period of approximately 5 months. There is significantly less temporal variation in the trihedral corner reflector response compared to the forest response only. The direct antenna coupling varies even less except during rain, where short but large variations in direct coupling occur. These results suggest that the instrument’s measurement characteristics are stable enough in time to measure temporal variations occurring in the forest backscatter over long timescales.*

2014). This error can be corrected for by applying a phase shift on the complex range profile such that the reflected power peak corresponding to the corner reflector is at the at the correct range from the antenna.

The resolution in azimuth is determined by the antenna radiation beam width, which can be up to  $116^\circ$  depending on the polarisation. The response from trihedral corner reflector 1 therefore falls in the same resolution cell as the forest under observation. Nevertheless, the response from this resolution cell still shows little variation in time as shown in Figure 3.6, indicating that the instrument measurement characteristics are stable in time.

## 3.6 Analysis Methods

### Backscatter

Time series of backscatter provide information about how the forest backscatter is affected by varying environmental parameters at different timescales and the effect that these environmental parameters have on estimates from backscatter-based forest parameter estimation models using SAR data. Backscatter can be estimated from a range interval of interest in a complex range profile  $r_{ij}(n)$  by treating the absolute square of this range profile as the  $R^4 P_r / P_t$  term in the radar equation. This gives

$$\sigma_{ij} = \frac{E}{N\lambda^2} \sum_{n=n_1}^{n_2} |r_{ij}(n)|^2 \quad (3.3)$$

where  $E$  is a magnitude calibration factor from the reference cable and direct coupling peak and  $\lambda$  is the wavelength in free space at the centre frequency  $f_c$ . Even though the backscatter is not calibrated in an absolute radiometric sense, the  $\lambda$  factor allows comparisons between frequency bands. The range indices  $n_1$  and  $n_2$  are the start and end indices of the range interval of interest. This interval should be chosen such that it includes responses throughout the entire forest height and such that the incidence angle range is similar to that used for spaceborne SARs.

### Temporal coherence

The temporal coherence gives a measure of the similarity of radar observations separated by a time interval  $\Delta t$ . Time series of the temporal coherence provide information on the length of temporal baselines that are suitable for repeat-pass SAR interferometry and tomography and how the coherence is affected by environmental parameters at different timescales. The first, reference measurement must be taken during *normal* conditions which can be considered to be dry, unfrozen, low wind speed conditions. The temporal coherence between two range profiles taken at times  $t = 0$  and  $t = \Delta t$  can be estimated by (Touzi et al. 1999)

$$\gamma_{ij} = \frac{\sum_{n=n_1}^{n_2} r_{ij}^0(n) \cdot r_{ij}^{\Delta t}(n)^*}{\sqrt{\sum_{n=n_1}^{n_2} |r_{ij}^0(n)|^2 \cdot \sum_{n=n_1}^{n_2} |r_{ij}^{\Delta t}(n)|^2}} \quad (3.4)$$

The magnitude and phase of  $\gamma_{ij}$  are the complex correlation coefficient and average phase shift respectively between the range intervals of interests between the two range profiles. Only the temporal coherence magnitude is investigated in this thesis.

### Tomography

Vertical backscattering profiles provide information on the vertical distribution of forest backscatter, how it varies over time and how this distribution responds to environmental changes. A complex-valued tomographic image with pixels at positions in a 2-dimensional vertical plane denoted by  $\mathbf{p}$  can be reconstructed through back-projection as

$$I(\mathbf{p}) = \sum_i \sum_j W_{El}(i, j) R_i(\mathbf{p}) R_j(\mathbf{p}) \tilde{s}_{ij} \left( \frac{R_i(\mathbf{p}) + R_j(\mathbf{p})}{2\Delta R} \right) \exp \left( -j2\pi f_c \frac{R_i(\mathbf{p}) + R_j(\mathbf{p})}{c_0} \right) \quad (3.5)$$

where  $R_i(\mathbf{p})$  and  $R_j(\mathbf{p})$  are the distances between the point  $\mathbf{p}$  on the two-dimensional vertical image plane and the receiving antenna  $i$  and transmitting antenna  $j$  respectively.  $W_{El}(i, j)$  is a window function for suppressing sidelobes in elevation, which was chosen to be the Taylor window. The range profile  $\tilde{s}_{ij}$  is the same as  $s_{ij}$  except interpolated to the range index in its argument. The exponential term at the end is a phase correction which is necessary because image reconstruction is done at baseband, easing the requirements on spatial sampling and reducing the processing time. The magnitude-squared values of the pixels, i.e.  $|I(\mathbf{p})|^2$ , form a vertical profile proportional to the forest backscatter.

In order to obtain a focused tomographic image, the relative phase shifts between the range profiles must be accurate to within a fraction of the wavelength. Due to residual phase errors in the data after phase calibration, a blurred image will be reconstructed unless these residual phase errors are compensated for. These residual phase errors arise due to inaccuracies in the trihedral corner reflector-based phase calibration. A similar defocusing problem occurs in airborne SARs due to measurement inaccuracies of the inertial measurement unit and Global Positioning System (Fornaro 1999; Fornaro, Franceschetti, and Perna 2005), which is solved using an autofocus algorithm.

In metric-based autofocus algorithms, the residual phase errors are estimated by maximising a particular image sharpness metric evaluated on the image intensity (Morrison, Do, and Munson 2007). In this experiment, this was done by optimising a vector of phase corrections  $\Phi$  for maximum tomographic image contrast, which is a popular approach for SAR autofocus (Schulz 2007). A single image involves contributions from 5 transmitting and 5 receiving antennas, giving 10 phase shift corrections to estimate. But only the relative phases affect the image sharpness, therefore one of the phase errors was set to 0 to serve as a reference phase. The phase correction vector  $\Phi$  therefore consists of nine phase correction elements, requiring an optimisation over a nine-dimensional parameter space. Image contrast can be maximised by minimising the image entropy  $H(\Phi)$ . The optimisation problem for finding the optimal phase corrections  $\hat{\Phi}$  can be expressed as

$$\hat{\Phi} = \arg \min_{\Phi} H(\Phi) \quad (3.6)$$

where the entropy is defined as

$$H(\Phi) = - \sum_{\mathbf{p}} P(\mathbf{p}, \Phi) \ln P(\mathbf{p}, \Phi) \quad (3.7)$$

with normalised pixel intensity  $P(\mathbf{p}, \Phi) = |I(\mathbf{p}, \Phi)|^2 / \sum_{\mathbf{p}} |I(\mathbf{p}, \Phi)|^2$ .  $I(\mathbf{p}, \Phi)$  is the complex tomogram reconstructed through back-projection after applying the phase shifts  $\Phi$  to the range profiles. The cost function  $H(\Phi)$  contains many local minima due to interference patterns arising from constructive and destructive interference. The optimisation was therefore carried out by firstly running a particle swarm optimisation and then refined through an interior-point approach to constrained optimisation as implemented in the `fmincon` function in Matlab. Figure 3.7 shows a C-band tomographic profile before and after autofocus.

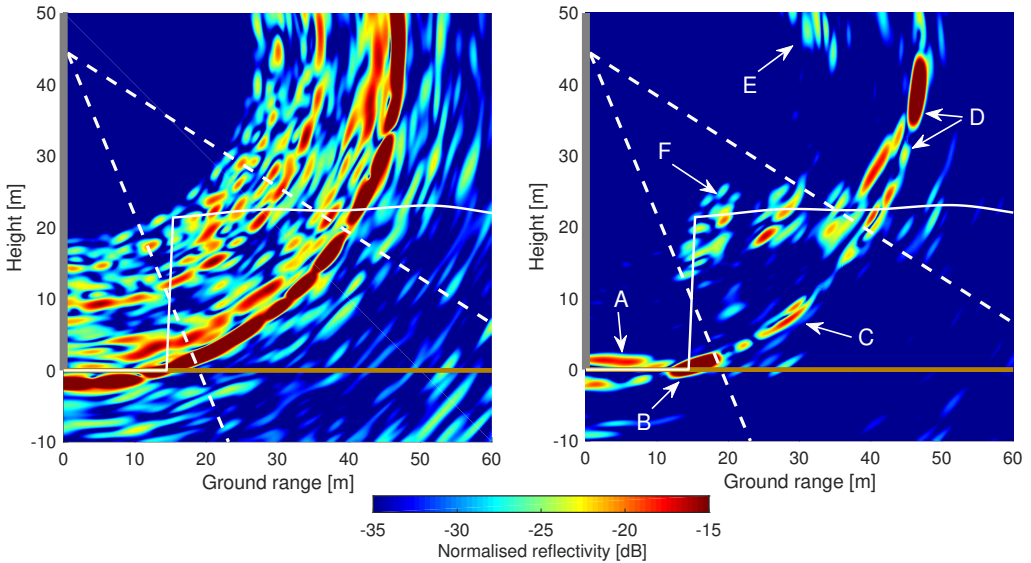


Figure 3.7. Example of tomographic reconstructions of C-band VV-polarised measurements without autofocus (left) and after autofocus (right) through maximisation of image sharpness. The dashed white lines show the  $-3$  dB antenna gain boundaries in elevation extending from the antenna array. The grey line indicates the position of the tower and the solid white line indicates the 95th percentile of an airborne lidar height estimates acquired in 2014, which is a measure of canopy height. The autofocused image shows several features: A=ground reflection, B=response from trihedral corner 4, C=sidelobe of corner reflector response, D=ambiguous response of the corner reflector and ground, E=ambiguous response of the forest and F=the desired forest response. Only the upper canopy contributes to the tomographic image since the C-band microwave radiation does not reach the stems and ground.

# 4

## Summary of Appended Papers

### **4.1 Paper A: Design and Implementation of the BorealScat Radar Instrument**

This report details the design and implementation of the BorealScat radar instrument and is based on the BorealScat Campaign Implementation Plan delivered to ESA in 2017. This document covers the technical details of the radar instrument design, including tomographic simulations of the antenna array performance and component selection. Ancillary data, the data collection scheme, data products and analysis methods are also described.

### **4.2 Paper B: Multi-port Vector Network Analyzer Radar for Tomographic Forest Scattering Measurements**

In September 2017 the C-band upgrade of BorealScat's radar instrument was complete. In this paper, the experimental setup is described, design issues are discussed and the signal processing steps are described. The first tomographic reconstructions from BorealScat data are demonstrated at P-, L- and C-band for the HH, HV and VV polarisations. Tomograms from the multi-port VNA measurements are compared to tomograms reconstructed from replicated 2-port VNA measurements using mechanical relays to route VNA ports to antennas. This was done to determine whether the shorter measurement sequence, made possible by the 20-port VNA, results in better tomographic imaging quality when the forest is moving due to wind during tomography measurements. Significant improvements in image quality were obtained for the multi-port VNA measurements at C-band for the measurements acquired during an average wind speed of 6 m/s. L-band tomograms showed minor improvements in image reconstruction quality for the multi-port VNA measurements while P-band results did not significantly differ from the 2-port VNA measurement results, as long as the same autofocus phase corrections are used.

### **4.3 Paper C: Temporal Survey of P- and L-band Polarimetric Backscatter in Boreal Forests**

In this paper, P- and L-band backscatter time series from January to August 2017 were analysed. During winter, large drops in backscatter (4 to 10 dB) were observed at both bands and all polarisations as the air temperature dropped below 0°C. This was attributed to a decrease in dielectric constant due to both frozen soil and frozen trunk moisture. During the spring/summer growing season, the P-band backscatter exhibited diurnal variations, along with temperature and

VPD. But the diurnal variations did not seem to originate from changing stem water content due to a diurnally varying VPD. Instead, it seemed to occur due to diurnal variations in wind speed. As the trees tilted due to wind, the dominating double-bounce mechanism was disturbed, lowering the co-polarised backscatter and increasing the cross-polarised backscatter. At L-band only an increase in HV backscatter was observed during windy times. Backscatter variations on timescales of days to weeks were observed that appeared to be due to a very high VPD and little rainfall, resulting in water stress in the trees. This was especially apparent at HH for both frequency bands.

Temporal coherence time series at P- and L-band extending over a two-month period in the summer of 2017 were also analysed. Co-polarised P-band temporal coherence was high ( $>0.9$ ) during the entire two month period, except during windy periods. HV coherence was high during the first month, after which it dropped after a period of water stress. P-band coherence was highest during night and early morning time when the wind speed was low, which are the most suitable times for repeat-pass observations by BIOMASS. L-band coherence was low after the first few hours of the reference measurement, strongly discouraging repeat-pass SAR observations at L-band.

# 5

## Conclusions and Future Work

The work in this thesis involved the design and implementation of the BorealScat campaign, an experiment for radar measurements of temporal variation in a boreal forest. The first backscatter and temporal coherence time series were analysed over a data collection interval duration of several months with widely varying environmental conditions and the first vertical backscattering profiles were successfully reconstructed. New information was revealed about how radar observables are affected by environmental parameters and our understanding of electromagnetic scattering mechanism in boreal forests was improved by this work.

The measurement results analysed thus far come from a very small portion of the full volume of collected data, and data collection will continue into the future. The analyses in this thesis can be refined and better calibration schemes can be done, resulting in better estimates of backscatter and coherence. Newly installed corner reflectors and new airborne SAR data over the site will facilitate an absolute radiometric calibration of the instrument. Time series of tomographic images will reveal temporal changes in the the distribution of forest backscatter and temporal coherence with height. Improved moisture sensors will give more information about the effect of soil and stem moisture on SAR observables. The BorealScat radar instrument also features measurements at UHF-band (614 - 670 MHz), for which the data is thus far unexplored. Finally, the information gained in this experiment should be incorporated into forward and inverse models of forest variables for reducing the unwanted effects of temporal variation on estimates using SAR data.



## References

- Ackermann, N (2015). *Growing Stock Volume Estimation in Temperate Forested Areas Using a Fusion Approach with SAR Satellites Imagery*. Springer International Publishing, p. 156.
- Albinet, C., P. Borderies, N. Floury, et al. (2016). Measure of temporal variation of P-band radar cross section and temporal coherence of a temperate tree. *IEEE Transactions on Geoscience and Remote Sensing*, vol. 54, no. 11, pp. 6255–6264.
- Albinet, C., P. Borderies, T. Koleček, et al. (2012). TropiSCAT: A ground based polarimetric scatterometer experiment in tropical forests. *IEEE Journal of Selected Topics in Applied Earth Observations and Remote Sensing*, vol. 5, no. 3, pp. 1060–1066.
- Albinet, C., T. Koleček, et al. (2015). First results of AfriScat, a tower-based radar experiment in African forest. *International Geoscience and Remote Sensing Symposium (IGARSS), Milan, Italy, 10-15 July 2016*, pp. 5356–5358.
- Askne, J. I. H., J. E. S. Fransson, et al. (2013). Model-based biomass estimation of a hemi-boreal forest from multitemporal TanDEM-X acquisitions. *Remote Sensing*, vol. 5, no. 11, pp. 5574–5597.
- Askne, J. I. H., M. J. Soja, and L. M. H. Ulander (2017). Biomass estimation in a boreal forest from TanDEM-X data, lidar DTM, and the interferometric water cloud model. *Remote Sensing of Environment*, vol. 196, pp. 265–278.
- Bamler, R. and P. Hartl (1998). Synthetic aperture radar interferometry. *Inverse Problems*, vol. 14, no. 4, R1–R54.
- Belcher, D. P. and N. C. Rogers (2009). Theory and simulation of ionospheric effects on synthetic aperture radar. *IET Radar, Sonar and Navigation*, vol. 3, no. 5, pp. 541–551.
- Billingsley, J. B. (2002). *Low-Angle Radar Land Clutter-Measurements and Empirical Models*. William Andrew Publishing/Noyes Publishing, Norwich.
- Borderies, P. et al. (2013). TropiSCAT: Final report. *European Space Agency (ESA), Paris, France, Tech. Rep. Contract No. 4000103506/11/NL/CT/FK*.
- Bradshaw, C. J. A. and I. G. Warkentin (2015). Global estimates of boreal forest carbon stocks and flux. *Global and Planetary Change*, vol. 128, pp. 24–30.
- Bradshaw, C. J. A., I. G. Warkentin, and N. S. Sodhi (2009). Urgent preservation of boreal carbon stocks and biodiversity. *Trends in Ecology & Evolution*, vol. 24, no. 10, pp. 541–548.
- Chirici, G., S. Winter, and R. E. McRoberts (2011). *National forest inventories: Contributions to forest biodiversity assessments*. Vol. 20. Springer Science & Business Media.
- Cloude, S. R. (2006). Polarization coherence tomography. *Radio Science*, vol. 41, no. 4, RS4017.
- Cumming, I. G and F. H Wong (2006). *Digital Signal Processing of Synthetic Aperture Radar Data: Algorithms and Implementation*. Artech House, Incorporated, Norwood.
- Dinh, H. T. M., S. Tebaldini, F. Rocca, T. Koleček, et al. (2013). Ground-based array for tomographic imaging of the tropical forest in P-band. *IEEE Transactions on Geoscience and Remote Sensing*, vol. 51, no. 8, pp. 4460–4472.
- Dinh, H. T. M., S. Tebaldini, F. Rocca, and T. Le Toan (2015). The Impact of Temporal Decorrelation on BIOMASS Tomography of Tropical Forests. *IEEE Geoscience and Remote Sensing Letters*, vol. 12, no. 6, pp. 1297–1301.

- Dobson, M. C. et al. (1992). Dependence of Radar Backscatter on Coniferous Forest Biomass. *IEEE Transactions on Geoscience and Remote Sensing*, vol. 30, no. 2, pp. 412–415.
- Drake, J. B. et al. (2002). Sensitivity of large-footprint lidar to canopy structure and biomass in a neotropical rainforest. *Remote Sensing of Environment*, vol. 81, no. 2-3, pp. 378–392.
- ESA (2012). *Report for Mission Selection: BIOMASS, ESA SP-1324/1 (3 volume series)*. European Space Agency, Noordwijk, The Netherlands.
- Fornaro, G. (1999). Trajectory deviations in airborne SAR: Analysis and compensation. *IEEE Transactions on Aerospace and Electronic Systems*, vol. 35, no. 3, pp. 997–1009.
- Fornaro, G., G. Franceschetti, and S. Perna (2005). Motion compensation errors: Effects on the accuracy of airborne SAR images. *IEEE Transactions on Aerospace and Electronic Systems*, vol. 41, no. 4, pp. 1338–1352.
- Fransson, J. E. S., F. Walter, and L. M. H. Ulander (2000). Estimation of forest parameters using CARABAS-II VHF SAR data. *IEEE Transactions on Geoscience and Remote Sensing*, vol. 38, no. 2, pp. 720–727.
- GCOS (2016). *The Global Observing System for Climate: Implementation Needs, GCOS-200*. World Meteorological Organization, Geneva.
- Hajnsek, I. et al. (2008). BioSAR 2007: Technical assistance for the development of airborne SAR and geophysical measurements during the BioSAR 2007 experiment: Final report. *European Space Agency (ESA), Paris, France, Tech. Rep. Contract No. 20755/07/NL/CB*.
- Hajnsek, I. et al. (2010). BioSAR 2008: Technical assistance for the development of airborne SAR and geophysical measurements during the BioSAR 2008 experiment: Final report. *European Space Agency (ESA), Paris, France, Tech. Rep. Contract No. 22052/08/NL/CT*.
- Houghton, R. A., F. Hall, and S. J. Goetz (2009). Importance of biomass in the global carbon cycle. *Journal of Geophysical Research: Biogeosciences*, vol. 114, no. 3.
- Hussin, Yousif Ali, Robin M. Reich, and Roger M. Hoffer (1991). Estimating slash pine biomass using radar backscatter. *IEEE Transactions on Geoscience and Remote Sensing*, vol. 29, no. 3, pp. 427–431.
- Hyde, Peter et al. (2007). Exploring LiDAR–RaDAR synergy—predicting aboveground biomass in a southwestern ponderosa pine forest using LiDAR, SAR and InSAR. *Remote Sensing of Environment*, vol. 106, no. 1, pp. 28–38.
- IEEE (2003). IEEE Standard Letter Designations for Radar-Frequency Bands. *IEEE Std 521-2002 (Revision of IEEE Std 521-1984)*, pp. 1–3.
- Israelsson, H., J. I. H. Askne, and R. Sylvander (1994). Potential of SAR for forest bole volume estimation. *International Journal of Remote Sensing*, vol. 15, no. 14, pp. 2809–2826.
- Israelsson, H., L. M. H. Ulander, et al. (1997). Retrieval of forest stem volume using VHF SAR. *IEEE Transactions on Geoscience and Remote Sensing*, vol. 35, no. 1, pp. 36–40.
- JAXA (2017). *ALOS-2 Basic Observation Scenario, Second Edition Rev .A*. JAXA/ALOS-2 Project.
- Krieger, G. et al. (2007). TanDEM-X: A satellite formation for high-resolution SAR interferometry. *IEEE Transactions on Geoscience and Remote Sensing*, vol. 45, no. 11, pp. 3317–3340.
- Le Quéré, C. et al. (2016). Global Carbon Budget 2016. *Earth System Science Data*, vol. 8, no. 2.
- Le Toan, T. et al. (1992). Relating Forest Biomass to SAR Data. *IEEE Transactions on Geoscience and Remote Sensing*, vol. 30, no. 2, pp. 403–411.
- Lee, J. and E. Pottier (2009). *Polarimetric radar imaging: from basics to applications*. CRC press.

- Marklund, L. G. (1988). *Biomassfunktioner för tall, gran och björk i Sverige*. Tech. rep. 45. Institutionen för skogstaxering, Sveriges lantbruksuniversitet, Umeå, Sweden.
- Mauseth, J. D. (2012). *Plants and people*. Jones & Bartlett Publishers.
- McDonald, K. C., R. Zimmermann, and J. S. Kimball (2002). Diurnal and spatial variation of xylem dielectric constant in Norway spruce (*Picea abies* [L.] Karst.) as related to microclimate, xylem sap flow, and xylem chemistry. *IEEE Transactions on Geoscience and Remote Sensing*, vol. 40, no. 9, pp. 2063–2082.
- Moreira, A. et al. (2015). Tandem-L: A highly innovative bistatic SAR mission for global observation of dynamic processes on the Earth's surface. *IEEE Geoscience and Remote Sensing Magazine*, vol. 3, no. 2, pp. 8–23.
- Morrison, R. L., M. N. Do, and D. C. Munson (2007). SAR image autofocus by sharpness optimization: A theoretical study. *IEEE Transactions on Image Processing*, vol. 16, no. 9, pp. 2309–2321.
- Narayanan, R. M., D. W. Doerr, and D. C. Rundquist (1992). Temporal decorrelation of X-band backscatter from wind-influenced vegetation. *IEEE Transactions on Aerospace and Electronic Systems*, vol. 28, no. 2, pp. 404–412.
- NASA (2015). *GEDI*. URL: <https://science.nasa.gov/missions/gedi/> (visited on 12/24/2017).
- Nelson, R., W. Krabill, and G. MacLean (1984). Determining forest canopy characteristics using airborne laser data. *Remote Sensing of Environment*, vol. 15, no. 3, pp. 201–212.
- Pan, Y. et al. (2011). A large and persistent carbon sink in the world's forests. *Science*, vol. 333, no. 6045, pp. 988–993.
- Petersson, H. (1999). *Biomassfunktioner för trädskott av tall, gran och björk i Sverige*. Tech. rep. Swedish University of Agricultural Sciences.
- Pielou, Evelyn C (1988). *The world of northern evergreens*. Cornell University Press.
- Pulliaainen, J. T., L. Kurvonen, and M. T. Hallikainen (1999). Multitemporal behavior of L- and C-band SAR observations of boreal forests. *IEEE Transactions on Geoscience and Remote Sensing*, vol. 37, no. 2, pp. 927–937.
- Ranson, K. J. and Guoqing S. (1994). Mapping biomass of a northern forest using multifrequency SAR data. *IEEE Transactions on Geoscience and Remote Sensing*, vol. 32, no. 2, pp. 388–396.
- Rawat, T. K. (2015). *Digital Signal Processing*. Oxford University Press.
- UN-REDD, PNG (2011). UN collaborative programme on reducing emissions from deforestation and forest degradation in developing countries. *National programme document. Papua New Guinea*.
- Regan, A., P. Silvestrin, and D. Fernandez (2016). Sentinel convoy: Synergetic earth observation with satellites flying in formation with European operational missions. *European Space Agency, (Special Publication) ESA SP*, vol. SP-740.
- Reigber, A. and A. Moreira (2000). First demonstration of airborne SAR tomography using multibaseline L-band data. *IEEE Transactions on Geoscience and Remote Sensing*, vol. 38, no. 5, pp. 2142–2152.
- Richards, M. A. (2014). *Fundamentals of Radar Signal Processing, Second Edition*. 2nd ed. McGraw-Hill Education.
- Richards, M. A., J. A. Scheer, and W. A. Holm (2010). *Principles of modern radar: Basic principles*. SciTech Publishing Incorporated.

- Rignot, E., J. Way, and L. Viereck (1994). Radar estimates of aboveground biomass in boreal Forests of interior Alaska. *IEEE Transactions on Geoscience and Remote Sensing*, vol. 32, no. 5, pp. 1117–1124.
- Rott, H. et al. (2017). “SESAME: A single-pass interferometric Sentinel-1 companion SAR mission for monitoring geo- and biosphere dynamics”. *2017 IEEE International Geoscience and Remote Sensing Symposium (IGARSS), Fort Worth, USA, 23-28 July 2017*, pp. 107–110.
- Saatchi, S. et al. (2007). Estimation of forest fuel load from radar remote sensing. *IEEE Transactions on Geoscience and Remote Sensing*, vol. 45, no. 6, pp. 1726–1740.
- Sandberg, G., L. M. H. Ulander, J. E. S. Fransson, et al. (2011). L- and P-band backscatter intensity for biomass retrieval in hemiboreal forest. *Remote Sensing of Environment*, vol. 115, no. 11, pp. 2874–2886.
- Sandberg, G., L. M. H. Ulander, J. Wallerman, et al. (2014). Measurements of forest biomass change using P-band synthetic aperture radar backscatter. *IEEE Transactions on Geoscience and Remote Sensing*, vol. 52, no. 10, pp. 6047–6061.
- Santoro, M., Leif E. B. Eriksson, and J. E. S. Fransson (2015). Reviewing ALOS PALSAR backscatter observations for stem volume retrieval in Swedish forest. *Remote Sensing*, vol. 7, no. 4, pp. 4290–4317.
- Santoro, M., J. E. S. Fransson, et al. (2009). Signatures of ALOS PALSAR L-band backscatter in Swedish forest. *IEEE Transactions on Geoscience and Remote Sensing*, vol. 47, no. 12, pp. 4001–4019.
- Schulz, T. J. (2007). Optimal sharpness function for SAR autofocus. *IEEE Signal Processing Letters*, vol. 14, no. 1, pp. 27–30.
- Sephton, Tony and Alex Wishart (2013). TOPOLEV and C-PARAS. *Distributed Space Missions for Earth System Monitoring*. Ed. by Marco D’Errico. New York, NY: Springer New York, pp. 473–508.
- Shteinshleiger, V. B. et al. (1997). Obtaining high resolution in transionospheric space-borne VHF-band SAR for Earth remote sensing. *IEE Conference Publication*, no. 449, pp. 268–272.
- Shvidenko, A. et al. (2010). Can the uncertainty of full carbon accounting of forest ecosystems be made acceptable to policymakers? *Climatic Change*, vol. 103, no. 1-2, pp. 137–157.
- Smith-Jonforsen, G., L. M. H. Ulander, and X. Luo (2005). Low VHF-band backscatter from coniferous forests on sloping terrain. *IEEE Transactions on Geoscience and Remote Sensing*, vol. 43, no. 10, pp. 2246–2260.
- Smith, G. and L. M. H. Ulander (2000). A model relating VHF-band backscatter to stem volume of coniferous boreal forest. *IEEE Transactions on Geoscience and Remote Sensing*, vol. 38, no. 2, pp. 728–740.
- Soja, M. J., H. J. Persson, and L. M. H. Ulander (2015). Estimation of forest biomass from two-level model inversion of single-pass InSAR data. *IEEE Transactions on Geoscience and Remote Sensing*, vol. 53, no. 9, pp. 5083–5099.
- Soja, M. J., G. Sandberg, and L. M. H. Ulander (2013). Regression-based retrieval of boreal forest biomass in sloping terrain using P-band SAR backscatter intensity data. *IEEE Transactions on Geoscience and Remote Sensing*, vol. 51, no. 5, pp. 2646–2665.
- Sparks, J. P., Gaylon S. Campbell, and A. R. Black (2001). Water content, hydraulic conductivity, and ice formation in winter stems of *Pinus contorta*: a TDR case study. *Oecologia*, vol. 127, no. 4, pp. 468–475.

- Stephens, B. B. et al. (2007). Weak northern and strong tropical land carbon uptake from vertical profiles of atmospheric CO<sub>2</sub>. *Science*, vol. 316, no. 5832, pp. 1732–1735.
- Torgovnikov, G. (1993). *Dielectric properties of wood and wood-based materials*. Springer Science & Business Media.
- Torres, R. et al. (2012). GMES Sentinel-1 mission. *Remote Sensing of Environment*, vol. 120, pp. 9–24.
- Torres, R. et al. (2017). Sentinel-1 SAR system and mission. *2017 IEEE Radar Conference, Seattle, USA, 8-12 May 2017*, pp. 1582–1585.
- Touzi, R. et al. (1999). Coherence estimation for SAR imagery. *IEEE Transactions on Geoscience and Remote Sensing*, vol. 37, no. 1, pp. 135–149.
- Ulaby, F. T. et al. (2014). *Microwave radar and radiometric remote sensing*. University of Michigan Press Ann Arbor.
- Ulander, L. M. H. et al. (2011). BioSAR 2010: Technical assistance for the development of airborne SAR and geophysical measurements during the BioSAR 2010 experiment: Final report. *European Space Agency (ESA), Paris, France, Tech. Rep. Contract No. 4000102285/10/NL/JA/ef*.
- Ulander, L. M. H. et al. (2016). Borealscat: A tower experiment for understanding temporal changes in P- and L-band backscattering from a Boreal forest. *European Space Agency, (Special Publication) ESA SP*, vol. SP-740.
- Van Laar, A. and A. Alparslan (2007). *Forest mensuration*. Vol. 13. Springer Science & Business Media.
- Way, J. et al. (1990). The effect of changing environmental conditions on microwave signatures of forest ecosystems: Preliminary results of the March 1988 Alaskan aircraft SAR experiment. *International Journal of Remote Sensing*, vol. 11, no. 7, pp. 1119–1144.
- Wolfe, J. and G. Bryant (2001). Cellular cryobiology: Thermodynamic and mechanical effects. *International Journal of Refrigeration*, vol. 24, no. 5, pp. 438–450.
- Wu, S. T. (1987). Potential Application of Multipolarization SAR for Pine-Plantation Biomass Estimation. *IEEE Transactions on Geoscience and Remote Sensing*, vol. 25, no. 3, pp. 403–409.
- Zebker, H. A. and J. Villasenor (1992). Decorrelation in interferometric radar echoes. *IEEE Transactions on Geoscience and Remote Sensing*, vol. 30, no. 5, pp. 950–959.